



Universiteit
Leiden
The Netherlands

Applicator visualization using ultrashort echo time MRI for high-dose-rate endorectal brachytherapy

Ende, R.P.J. van den; Ercan, E.; Keesman, R.; Kerkhof, E.M.; Marijnen, C.A.M.; Heide, U.A. van der

Citation

Ende, R. P. J. van den, Ercan, E., Keesman, R., Kerkhof, E. M., Marijnen, C. A. M., & Heide, U. A. van der. (2020). Applicator visualization using ultrashort echo time MRI for high-dose-rate endorectal brachytherapy. *Brachytherapy*, 19(5), 618-623.
doi:10.1016/j.brachy.2020.06.010

Version: Publisher's Version
License: [Creative Commons CC BY-NC-ND 4.0 license](#)
Downloaded from: <https://hdl.handle.net/1887/3182837>

Note: To cite this publication please use the final published version (if applicable).

Physics

Applicator visualization using ultrashort echo time MRI for high-dose-rate endorectal brachytherapy

Roy P.J. van den Ende^{1,*}, Ece Ercan², Rick Keesman³, Ellen M. Kerkhof¹,
Corrie A.M. Marijnen^{1,3}, Uulke A. van der Heide^{1,3}

¹Department of Radiation Oncology, Leiden University Medical Center, Leiden, the Netherlands

²C.J. Gorter Center for High Field MRI, Department of Radiology, Leiden University Medical Center, Leiden, the Netherlands

³Department of Radiation Oncology, The Netherlands Cancer Institute, Amsterdam, the Netherlands

ABSTRACT

PURPOSE: The individual channels in an endorectal applicator for high-dose-rate endorectal brachytherapy are not visible on standard MRI sequences. The aim of this study was to test whether an ultrashort echo time (UTE) MRI sequence could be used to visualize the individual channels to enable MR-only treatment planning for rectal cancer.

METHODS AND MATERIALS: We used a radial three-dimensional (3D) UTE pulse sequence and acquired images of phantoms and two patients with rectal cancer. We rigidly registered a UTE image and CT scan of an applicator phantom, based on the outline of the applicator. One observer compared channel positions on the UTE image and CT scan in five slices spaced 25 mm apart. To quantify geometric distortions, we scanned a commercial 3D geometric quality assurance phantom and calculated the difference between detected marker positions on the UTE image and corresponding marker positions on two 3D T₁-weighted images with opposing readout directions.

RESULTS: On the UTE images, there is sufficient contrast to discern the individual channels. The difference in channel positions on the UTE image compared with the CT was on average -0.1 ± 0.1 mm (left-right) and 0.1 ± 0.3 mm (anteroposterior). After rigid registration to the 3D T₁-weighted sequences, the residual 95th percentile of the geometric distortion inside a 550-mm-diameter sphere was 1.0 mm (left-right), 0.9 mm (anteroposterior), and 0.9 mm (craniocaudal).

CONCLUSIONS: With a UTE sequence, the endorectal applicator and individual channels can be adequately visualized in both phantom and patients. The geometrical fidelity is within an acceptable range. © 2020 The Authors. Published by Elsevier Inc. on behalf of American Brachytherapy Society. This is an open access article under the CC BY-NC-ND license (<http://creativecommons.org/licenses/by-nc-nd/4.0/>).

Keywords: Rectal cancer; Brachytherapy; MRI; Ultrashort echo time

Introduction

For patients with rectal cancer, high-dose-rate endorectal brachytherapy (HDREBT) can be used to deliver high doses to the tumor while sparing the surrounding organs

at risk due to a steep dose gradient (1). HDREBT may be delivered using an intracavitary mold applicator set, such as the flexible eight-channel applicator (Elekta, Veenendaal, the Netherlands). Applicator reconstruction for the flexible eight-channel applicator is currently performed on CT (2,3) because the individual channels of the applicator are not visible on conventional MR images because of the short T₂-relaxation time of the applicator. However, CT suffers from limited soft-tissue contrast, which makes it challenging to delineate the target volume accurately (4,5). MRI is the primary imaging modality for tumor visualization because of its superior soft-tissue contrast, and it is therefore currently registered to CT imaging to aid in the tumor delineation on CT. However, acquiring both CT and MRI on the same day can be time consuming, and

Received 23 February 2020; received in revised form 8 June 2020; accepted 9 June 2020.

Financial disclosure: The authors report no proprietary or commercial interest in any product mentioned or concept discussed in this article. This work was supported by the Dutch Cancer Society/Alpe d'HuZes Fund, grant UL2013-6311.

* Corresponding author. Leiden University Medical Center, Department of Radiation Oncology, P.O. Box 9600, 2300 RC Leiden, the Netherlands. Tel.: +31715265539; fax: +31715266760.

E-mail address: r.p.j.van_den_ende@lumc.nl (R.P.J. van den Ende).

changes in applicator positioning between the scans may occur because of patient movement and/or differences in organ filling. An MRI-only approach in which applicator reconstruction, delineation of the target volume and organs at risk, and treatment planning are performed on MRI is therefore preferred.

MRI-only brachytherapy treatment planning is already the standard for cervical cancer in Europe (6). To perform applicator reconstruction on MRI, models of rigid applicators have been made available in commercial treatment planning systems, and these can be rigidly registered to the applicator on MR images. However, for nonrigid applicators such as the flexible endorectal applicator, such models are not available. In addition, because the individual channels of the flexible endorectal applicator are not visible on MRI, the rotation of the applicator cannot be determined because of its cylindrical shape. In brachytherapy for cervical cancer, dummy catheters can be used to aid in applicator reconstruction. The dummy catheter is filled with a fluid that produces high signal intensity on MRI. However, such dummy catheters are not available for the flexible endorectal applicator. As an alternative, an ultrashort echo time (UTE) sequence (7,8) may be used to visualize the applicator and the individual channels. UTE uses very short echo times on the order of <0.5 ms and allows visualization of materials with very short T_2 -relaxation times.

The aim of this study was to test if a UTE sequence can be used to visualize the individual channels within the flexible endorectal applicator for HDREBT treatment planning. To this end, we first evaluated the visibility of the individual channels in a phantom and determined the geometric fidelity of the UTE sequence. Finally, we acquired UTE images from two patients with rectal cancer with applicator in situ to evaluate the visibility of the individual channels in an applicator in situ.

Methods and materials

Applicator

We used a commercial intracavitary mold applicator (OncoSmart, Elekta, Veenendaal, The Netherlands). This is a flexible cylindrical applicator made of silicon with a diameter of 20 mm and a length of 280 mm. The applicator has eight channels radially spaced along its circumference, which allows for an asymmetric dose distribution (9).

UTE sequence

All MRI scans in this study were performed on a 3T scanner (Ingenia, Philips Healthcare, Best, The Netherlands). We used a three-dimensional (3D) stack of radials UTE pulse sequence for radial sampling of free induction decays, enabled by clinical science functionality under a research agreement. A cylindrical encoding scheme

was performed with radial sampling in-plane and cartesian sampling through-plane. Radial sampling was used as it allows for very short echo times in the order of <0.5 ms. The sequence is similar to the stack of spirals UTE sequence described in the study by Qian and Boada (10). For UTE excitation, a nonselective hard radiofrequency pulse was applied for a very short duration (0.05 ms) and was followed by a phase-encoding gradient in craniocaudal (CC) direction for slice encoding. Immediately after the phase-encoding gradient, a radial readout was performed to quickly sample the k-space in the two directions that are perpendicular to the slice direction. The radial k-space data acquisition started already during the ramp of the gradients (7). The scan parameters for the UTE sequences used for imaging the applicator phantom, the two patients, and the geometric quality assurance (QA) phantom are shown in Table 1. To ensure clinical feasibility, the scanning times for patients were kept less than 6 min.

Applicator phantom

To optimize and evaluate the UTE sequence for applicator visualization, we prepared a phantom. We first filled a box ($400 \times 300 \times 190$ mm³) halfway with agarose gel. The agarose gel consisted of 0.2 g of Dotarem 0.5 mM (Guerbet, Villepinte, France), 10 g of agar (A1296, Sigma-Aldrich, Saint Louis, MO), and 3 g of NaCl per liter water, aiming for a T_1 (spin-lattice relaxation time) of 1–2 s and a T_2 (spin-spin relaxation time) of >30 ms (11), which is on the same order of magnitude as the relaxation properties of human soft-tissue around the rectum. A balloon was placed around the applicator and subsequently filled with 20 cc of water with 5% Telebrix Gastro (Guerbet, Villepinte, France), as in our clinical procedure. The applicator was then placed on top of the first layer of agarose gel, and a second layer of agarose gel was applied to fill the box.

Individual channel visualization

To evaluate the visibility of the individual channels within the applicator, we acquired an axial UTE image of the phantom. To test whether the visualized channels on the UTE image actually represent the individual channels within the applicator, we acquired an axial CT scan (Brilliance Big Bore, Philips Healthcare, Best, The Netherlands) of the phantom (voxel size $0.63 \times 0.63 \times 1$ mm³, 120 kVp, tube current 346 mA, exposure time 887 ms). We performed a rigid registration of the CT scan to the UTE image based on the outline of the applicator using Elastix, a toolbox for intensity-based medical image registration (12). To determine channel positions, one observer manually aligned a two-dimensional template of the channel configuration on the UTE image and the registered CT scan in five slices spaced 25 mm apart. We then calculated the in-plane difference in channel positions between the UTE

Table 1

Scan parameters for the UTE sequences used for imaging the applicator phantom, the patients, and the geometric fidelity phantom

Parameter	Applicator phantom	Patient 1	Patient 2	Geometric QA phantom
Voxel size (mm ³)	1.0×1.0×2.5	1.0×1.0×3.5	0.98×0.98×2.5	1.94×1.94×1.94
Echo time (ms)	0.14	0.14	0.14	0.14
Repetition time (ms)	5.26	4.97	5.22	4.22
Acquisition grid	376×376×126	376×376×90	384×384×90	288×288×206
Field of view (mm ³)	376×376×315	376×376×315	376×376×225	560×560×400
Readout bandwidth (Hz/mm)	886	886	886	895
SENSE factor	1.4	1.4	1.4	1.0
Flip angle (deg)	10	10	10	10
Acquisition duration (s)	499	337	353	643

QA = quality assurance; UTE = ultrashort echo time.

image and the CT scan. To evaluate the visibility of the channels in a clinical setting, we acquired informed consent from two patients with rectal cancer undergoing HDREBT within a clinical trial. In addition to the MRI sequences acquired for HDREBT treatment planning, we acquired an additional axial UTE image for these two patients with the applicator in situ. As part of sequence optimization, we acquired a UTE image with a slice thickness of 3.5 mm in the first patient and a slice thickness of 2.5 mm in the second patient. For one slice in each UTE image, we determined the contrast-to-noise ratio ($CNR = |S_C - S_A|/\sigma$) of the channels relative to the applicator. Here, S_C and S_A are the average signal intensities of the channels and the applicator, respectively, and σ is the SD of the image noise. Average signal intensities were extracted from regions of interest of 2×2 mm placed on and between the channels. In a similar fashion, σ was estimated from signal intensity variations inside a region of interest in the balloon surrounding the applicator.

Geometric fidelity

To quantify geometric distortions, we acquired MRI images of a commercial 3D geometric QA phantom (Philips Healthcare, Best, The Netherlands) (13,14). The phantom was placed on the treatment table centered around the isocenter. It consists of seven plastic plates, placed 55 mm apart, each containing 276 spheres (markers) with a diameter of 10 mm filled with oil. Within each plate, the markers

are located on a grid with a spacing of 25 mm. In total, the phantom is 330-mm long and has a diameter of 500 mm.

To determine the actual position of the markers within the phantom, we used two axial 3D T_1 -weighted gradient-echo sequences (voxel size: $1.94 \text{ mm} \times 1.94 \text{ mm} \times 1.94 \text{ mm}$, field of view: $560 \times 560 \times 400 \text{ mm}^3$, echo time: 3.40 ms, repetition time: 6.90 ms, readout bandwidth: 828 Hz/mm) with opposing readout directions (anterior and posterior) to be able to correct for magnetic-field inhomogeneity. Subsequently, we acquired a UTE image with the same isotropic voxel size as the two axial 3D T_1 -weighted images (Table 1). The marker detection algorithm described in the study by Keesman et al. (13) was used to detect the markers, which produced lists of marker positions, one for each image.

To correct for magnetic-field inhomogeneity, the corresponding detected marker positions in the two 3D T_1 -weighted images were averaged. To assess the distortion of the averaged 3D T_1 -weighted marker positions, a regular reference grid (containing the ideal marker positions, defined according to the known geometry of the phantom) was rigidly registered per plate to the averaged 3D T_1 -weighted marker positions. Residuals between the averaged 3D T_1 -weighted marker positions and the registered reference grid ($ref_grid_{T_1-3D}$) were calculated.

To assess the geometric distortion of the UTE image relative to the 3D T_1 -weighted images, we calculated the residuals between detected markers in the UTE image and $ref_grid_{T_1-3D}$. The 5th, 50th, and 95th percentiles for

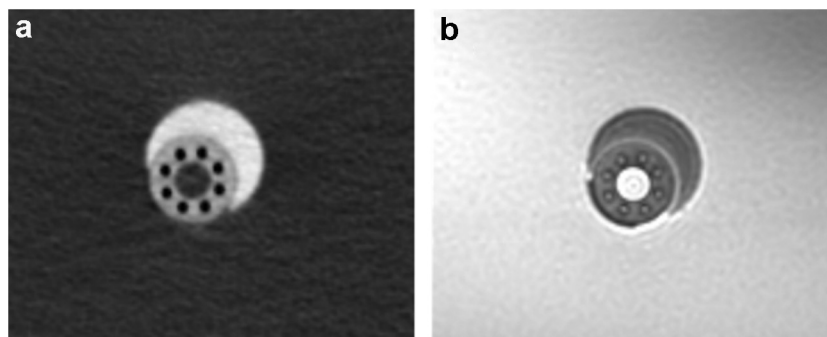


Fig. 1. Axial CT scan (a) and UTE MR image (b) of the applicator phantom containing the flexible endorectal applicator and a balloon placed around the applicator. UTE = ultrashort echo time.

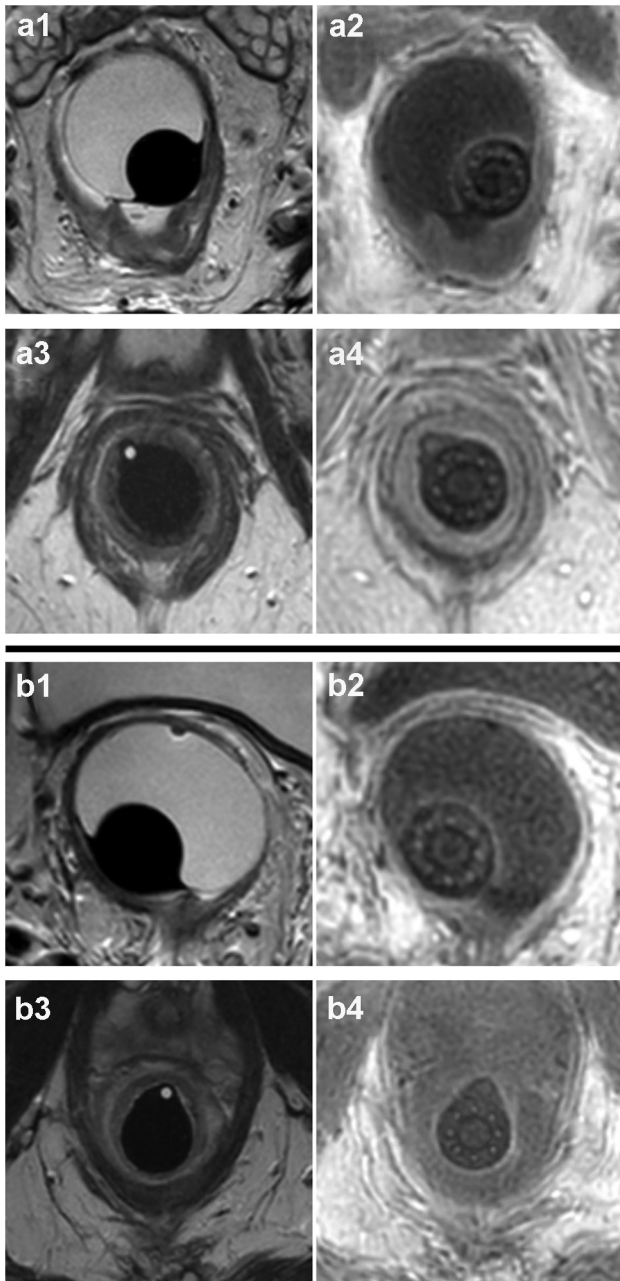


Fig. 2. Axial slices of T2-TSE images (a1, a3, b1, and b3) and UTE images (a2, a4, b2, and b4) in two patients (a and b) with the applicator in situ. UTE = ultrashort echo time.

the residuals are presented for various diameters of spherical volume (DSV) to evaluate the geometric fidelity for various distances from the isocenter.

Results

Individual channel visualization

On the UTE image that was acquired of the applicator phantom, the channels have sufficient contrast relative to

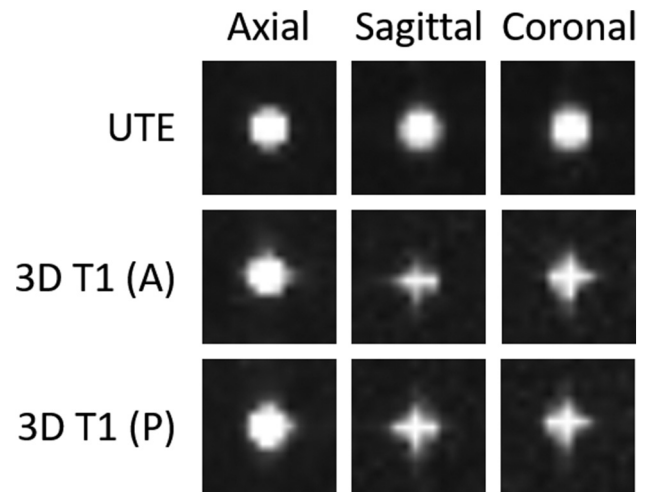


Fig. 3. Appearance of a single marker of the 3D geometric QA phantom in the axial, sagittal, and coronal plane on a UTE image and two 3D T₁-weighted images with opposing readout directions (A = anterior readout direction, P = posterior readout direction). UTE = ultrashort echo time; 3D = three-dimensional; QA = quality assurance.

the applicator itself to be able to discern the individual channels (Fig. 1). The difference in channel positions on the UTE image compared with the CT was on average -0.1 ± 0.1 mm (left-right (LR)) and 0.1 ± 0.3 mm (anteroposterior (AP)). In addition, individual channels are visible on the UTE patient images (Fig. 2). The CNR was calculated from the slices that contained the balloon (Fig. 2, A2 and B2). The CNR was 1.9 for patient 1 and 2.4 for patient 2.

Geometric distortion

In total, 1428 corresponding markers of the 1932 markers in the geometric QA phantom were detected by the marker detection algorithm in both the 3D T₁-weighted images and the UTE image. Marker appearance on the UTE image and the 3D T₁-weighted images with opposing readout directions is shown in Fig. 3. The mean and SD of the residuals between the averaged 3D T₁-weighted marker positions and $\text{ref_grid}_{\text{T1_3D}}$ was 0.01 ± 0.42 mm (LR), -0.03 ± 0.36 mm (AP), and 0.02 ± 0.33 mm (CC). The 95th percentile of the residuals was 0.81 mm (LR), 0.68 mm (AP), and 0.65 mm (CC) within a DSV of 550 mm, which includes all detected markers. In Fig. 4, the residuals are plotted as a function of distance to the isocenter in the LR, AP, and CC directions, respectively.

The mean and SD of the residuals between detected markers in the UTE image and $\text{ref_grid}_{\text{T1_3D}}$ were 0.46 ± 0.46 mm (LR), -1.69 ± 0.50 mm (AP), and 0.07 ± 0.48 mm (CC). This indicates a systematic shift, mostly in the AP direction. In a clinical scenario, a rigid registration is performed between the UTE image and an anatomical image based on the outline of the applicator to correct for any changes in patient and/or applicator

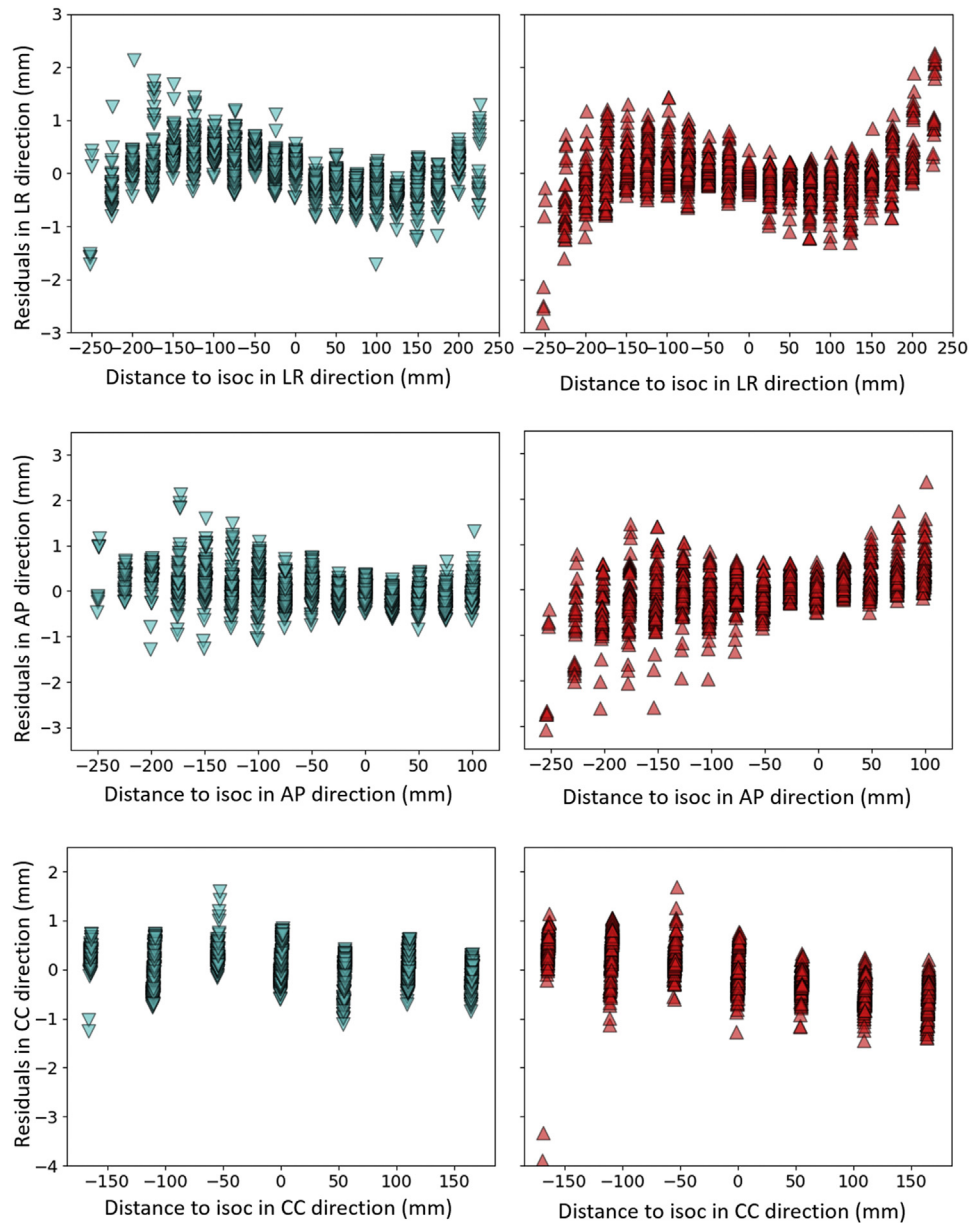


Fig. 4. Residuals of the average detected marker positions of the 3D T_1 -weighted images (blue) and residuals of detected markers in the UTE image (red) with respect to $ref_grid_{T_1-3D}$ in the LR, AP, and CC directions as a function of distance to isocenter (isoc) in the LR, AP, and CC directions, respectively. UTE = ultrashort echo time; 3D = three-dimensional; LR = left-right; AP = anteroposterior; CC = craniocaudal. (For interpretation of the references to color in this figure legend, the reader is referred to the Web version of this article.)

positioning that can occur within the scan session. To investigate effects of higher-order distortion patterns in the UTE image, we corrected this systematic shift by means of a global translation. Subsequently, we calculated the remaining residuals. The 5th, 50th, and 95th percentiles for these residuals within various DSVs are presented in Table 2. A 95th percentile of 1.0 mm or lower is observed in all directions within a DSV of 550 mm. The magnitude of the distortions increases with increasing distance from the isocenter. This can also be observed in Fig. 4, where the residuals are plotted as a function of distance to the isocenter in the LR, AP, and CC directions, respectively.

Discussion

Treatment planning for HDREBT for rectal cancer using the flexible endorectal applicator is currently not performed on MRI alone, as the individual channels within the applicator are not visible on MRI images. The aim of this study was to test if a UTE sequence can be used to visualize the individual channels within the flexible endorectal applicator for HDREBT treatment planning. We have shown that the individual channels are visible on UTE images, both in a phantom and in patients. The CNR of the channels and the applicator was higher in patient 2. This may be explained by a partial

Table 2

Measured residuals of detected marker positions in the UTE image relative to ref_grid_{T1_3D} in the LR, AP, and CC directions after rigid registration of the detected markers in the UTE image to ref_grid_{T1_3D}

DSV (mm)	Percentile	LR (mm)	AP (mm)	CC (mm)	No. of markers
100	5th	0.0	0.0	0.0	11
	50th	0.1	0.1	0.1	
	95th	0.2	0.4	0.7	
200	5th	0.0	0.0	0.0	121
	50th	0.1	0.1	0.2	
	95th	0.3	0.4	0.6	
300	5th	0.0	0.0	0.0	387
	50th	0.1	0.2	0.3	
	95th	0.3	0.4	0.7	
400	5th	0.0	0.0	0.0	862
	50th	0.1	0.2	0.3	
	95th	0.5	0.6	0.8	
550	5th	0.0	0.0	0.0	1428
	50th	0.2	0.3	0.3	
	95th	1.0	0.9	0.9	

UTE = ultrashort echo time; DSV = diameter of spherical volume; LR = left-right; AP = anteroposterior; CC = craniocaudal.

volume effect due to a difference in slice thickness, which was 3.5 mm for patient 1 and 2.5 mm for patient 2.

We observed a systematic shift of the detected marker positions in the UTE image relative to ref_grid_{T1_3D}, especially in the AP direction. In a clinical application, an anatomical image is used for delineation, while the UTE image would be used to visualize the individual channels within the applicator. A rigid registration would be performed based on the outline of the applicator and surrounding balloon, negating any systematic offsets. After correcting for the systematic shift, the 95th percentile of the residuals is 1.0 mm or lower in all directions within a DSV of 550 mm. In addition, within a volume that is typically of interest for applicator reconstruction (i.e., a DSV of 300 mm), the 95th percentile of the residuals was 0.3 mm (LR), 0.4 mm (AP), and 0.7 mm (CC), which is acceptable for HDREBT treatment planning.

In a UTE sequence, k-space data acquisition starts quickly after the radiofrequency excitation and is performed during the ramp-up of the gradients (7). This makes the UTE sequence prone to degraded image quality due to eddy currents and unbalanced hardware time delays, which lead to undesired k-space trajectory deviations (15). This could have contributed to the systematic shift we have observed. Although for our application it suffices to correct for this shift by using a rigid registration, different techniques can be used to measure the actual k-space trajectory to improve the image reconstruction (15–17).

Conclusions

The endorectal applicator and the individual channels can be adequately visualized using a UTE sequence in both a phantom and patients. After a rigid registration to an anatomical image, the geometric fidelity of the UTE

sequence is within an acceptable range. The UTE sequence is therefore suitable for HDREBT treatment planning.

Supplementary data

Supplementary data related to this article can be found at <https://doi.org/10.1016/j.brachy.2020.06.010>.

References

- [1] Vuong T, Richard C, Niazi T, et al. High dose rate endorectal brachytherapy for patients with curable rectal cancer. *Semin Colon Rectal Surg* 2010;21:115–119.
- [2] Vuong T, Devic S. High-dose-rate pre-operative endorectal brachytherapy for patients with rectal cancer. *J Contemp Brachytherapy* 2015;7:181–186.
- [3] Nout RA, Devic S, Niazi T, et al. CT-based adaptive high-dose-rate endorectal brachytherapy in the preoperative treatment of locally advanced rectal cancer: Technical and practical aspects. *Brachytherapy* 2016;15:477–484.
- [4] O'Neill BDP, Salerno G, Thomas K, et al. MR vs CT imaging: Low rectal cancer tumour delineation for three-dimensional conformal radiotherapy. *Br J Radiol* 2009;82:509–513.
- [5] Khoo VS, Joon DL. New developments in MRI for target volume delineation in radiotherapy. *Br J Radiol* 2006;79:2–15.
- [6] Pötter R, Haie-Meder C, Van Limbergen E, et al. Recommendations from gynaecological (GYN) GEC ESTRO working group (II): Concepts and terms in 3D image-based treatment planning in cervix cancer brachytherapy - 3D dose volume parameters and aspects of 3D image-based anatomy, radiation physics, radiobiology. *Radiother Oncol* 2006;78:67–77.
- [7] Holmes JE, Bydder GM. MR imaging with ultrashort TE (UTE) pulse sequences: Basic principles. *Radiography* 2005;11:163–174.
- [8] Bos C, Moerland MA, van den Brink J, et al. MR image guidance of brachytherapy needle placement: Potential of 2D ultrashort echo time imaging. *Int J Radiat Oncol* 2013;87:S671.
- [9] Poon E, Reniers B, Devic S, et al. Dosimetric characterization of a novel intracavitary mold applicator for 192Ir high dose rate endorectal brachytherapy treatment. *Med Phys* 2006;33:4515–4526.
- [10] Qian Y, Boada FE. Acquisition-weighted stack of spirals for fast high-resolution three-dimensional ultra-short echo time MR imaging. *Magn Reson Med* 2008;60:135–145.
- [11] Shen Y, Goerner FL, Snyder C, et al. T1 relaxivities of gadolinium-based magnetic resonance contrast agents in human whole blood at 1.5, 3, and 7T. *Invest Radiol* 2015;50:330–338.
- [12] Klein S, Staring M, Murphy K, et al. Elastix: a toolbox for intensity-based medical image registration. *IEEE Trans Med Imaging* 2010;29:196–205.
- [13] Keesman R, van de Lindt TN, Juan-Cruz C, et al. Correcting geometric image distortions in slice-based 4D-MRI on the MR-linac. *Med Phys* 2019;46:3044–3054.
- [14] Ranta I, Kemppainen R, Keyriläinen J, et al. Quality assurance measurements of geometric accuracy for magnetic resonance imaging-based radiotherapy treatment planning. *Phys Med* 2019;62:47–52.
- [15] Atkinson IC, Lu A, Thulborn KR. Characterization and correction of system delays and eddy currents for MR imaging with ultrashort echo-time and time-varying gradients. *Magn Reson Med* 2009;62:532–537.
- [16] Latta P, Starčuk Z, Gruwel MLH, et al. K-space trajectory mapping and its application for ultrashort Echo time imaging. *Magn Reson Imaging* 2017;36:68–76.
- [17] Kronthaler S, Rahmer J, Börner P, et al. Trajectory correction for ultrashort echo-time (UTE) imaging based on the measurement of the gradient impulse response function (GIRF) with a thin-slice method. *Proc Intl Soc Mag Reson Med* 2019;27.